A Survey of Gasoline Ameliorator, Methyl-Tert-Butyl Ether (MTBE) on Bovine Serum Albumin: A Spectroscopy and Molecular Dynamic Simulation Study

Ebrahim Shahmansoorian[1], Seyed-Mohammad Atyabi[2*], Parichehreh Yaghmaei[1], Faramarz Mehrnejad[3]**

[1]Department of biology, Faculty of Basic Sciences, Science and Research Branch, Islamic Azad University, Tehran, Iran
[2]Department of Pilot Nanobiotechnology, Pasteur Institute of Iran, Tehran, Iran
[3]Department of Life Science Engineering, Faculty of New Sciences and Technologies, University of Tehran, Tehran, Iran

Corresponding author: Seyed-Mohammad Atyabi, Department of Pilot Nanobiotechnology, Pasteur Institute of Iran, Tehran, Iran. Tel: +98- 2164112165, Fax: +98- 2166465132, E-mail: atyabi@pasteur.ac.ir

**Co-Corresponding author*: Faramarz Mehrnejad, Department of Life Science Engineering, Faculty of New Sciences and Technologies, University of Tehran, Tehran, Iran. Tel: +98-2186093285, Fax: +98-2188497324, E-mail: mehrnejad@ut.ac.ir

Background: Methyl-Tert-Butyl Ether (MTBE) as a gasoline modifier is frequently added to fuels and used in plenty of worldwide applications. MTBE biodegradation in groundwater occurs slowly and produces water miscibility; therefore, it causes diverse environmental and human health concerns.

Objectives: The interaction of MTBE with bovine serum albumin (BSA) as a model protein at physiological conditions is investigated to illustrate the possible interactions of MTBE with the body's proteins.

Materials and Methods: Uv–visible, fluorescence, circular dichroism (CD) spectroscopy methods, and molecular modeling were used to analyze the MTBE's effect on BSA structure and dynamics. The constant protein concentration and various MTBE contents were used for possible interactions.

Results: The protein structural analysis shows that MTBE binds to BSA via positive enthalpy and entropy via hydrophobic interactions. Molecular docking shows the participation of several amino acids in the MTBE-BSA interaction. The CD spectroscopy results show that the BSA structure was not changed in the MTBE concentrations utilized in the study. Molecular dynamics (MD) simulation results suggest that MTBE can slightly change protein structure in the last 50ns.

Conclusion: Comparing experimental and MD simulation results demonstrated that the BSA secondary structure was maintained in the low concentration of the MTBE. The entropy and enthalpy parameters asserted the hydrophobic interaction was the major force in the interaction between the BSA and MTBE.

Keyword: Bovine Serum Albumin; Methyl-Tert-Butyl Ether; Molecular Dynamics Simulation; Secondary Structure

1. Background

Methyl-tert-butyl ether is an organic compound with a chemical formulation of $(CH_3)_3COCH_3$. MTBE, also known as tert-butyl methyl ether, is a volatile, flammable, and colorless liquid. MTBE has been used as an oxygenating compound to improve gasoline octane levels since the late 1970s and replaced by the carcinogenic compounds of Tetraethyllead $(CH_3CH_2)_4Pb$. MTBE improves engine combustion efficiency while also lowering carbon monoxide, sulfur, ozone, and aromatic benzene emissions into the environment (1, 2). Yearly, above 20 million tons of MTBE is manufactured and used globally (3). It is not surprising to show that MTBE by physicochemical properties such as high-water solubility, high volatility, and slow biodegradability found in the environment as

a pollutant to enter atmosphere and groundwater via accidental leakage during production, transportation, and storage (4, 5). Therefore, exposure to this compound via inhalation or drinking water affects human health. In 1999 the California Environmental Protection Agency (Sacramento, CA, USA) and the US Environmental Protection Agency (EPA) classified MTBE as a possible human carcinogenic agent (6).

According to research, MTBE was shown to build in the bloodstream and breath, causing skin and eye irritation, diarrhea, vomiting, fever, cough, dizziness, tiredness, and headaches (7). Several studies confirmed that MTBE causes kidney and liver damage and makes leukemia and Leydig cells testicular tumors, especially in animals, mainly rodents (8-12). Despite many studies on cellular toxicity, few studies exist on MTBE's toxic effects at the molecular level or MTBE protein interactions. MTBE protein interactions (13,14). Proteins are the most important bioactive molecules in life; hence, a serum's reduction or rise in protein levels might be used as a key indicator for clinical diagnosis and health assessment. Furthermore, protein research with exogenous compounds such as contaminants is critical for a health assessment (15).

After quickly entering the bloodstream, MTBE interacts with the blood proteins (16, 17). One of the main soluble proteins in the circulatory system is serum albumin, with diverse physiological functions such as transporting many exogenous and endogenous molecules (18, 19). The protein-ligand interactions and binding processes are widely studied using serum albumin as a model protein. Thus, regarding 76% structural homology with human serum albumin (HSA), bovine serum albumin was used extensively for protein-ligand interactions (20, 21). BSA has three homolog domains; domain I, domain II and domain III, divided into nine loops (L1–L9) with 17 disulfide bonds. These loops formed a sequence of large-small-large loops and built a triplet in each domain. Each domain includes two subdomains, A and B. α-helix is a predominant BSA secondary structure (22).

2. Objectives

MTBE accumulation in the bloodstream and breath affects human health. As a result, the effects of MTBE on the structure of BSA were investigated using experimental methods such as fluorescence spectroscopy and circular dichroism (CD). The binding

of MTBE to the protein was also shown using molecular dynamics (MD) modeling.

3. Methods and Material

3.1. Materials
Bovine Serum Albumin (BSA) was purchased from Canada-Bioshop Company. Methyl-tert-butyl ether (MTBE) was prepared from ACROS organics. Phosphate Buffered Saline (PBS) was obtained from Bio Basic Company. All solutions were prepared with double-distilled water.

3.2. UV-Visible Spectroscopy
The UV-visible absorption spectra (200-700 nm) of BSA solution (2.25 μM) were performed in different concentrations of MTBE (0-9λ, each λ equal 8.3 μM), and it was recorded after zero and three-hour incubation at 37 °C. UV/Vis spectrometer Perkin Elmer measurements were carried out from 200 to 700 nm using a slit of 5 nm and a scan speed of 250 nm/min with jacketed cell holders. All experiments were run in phosphate-buffered saline containing 2.7 mM potassium chloride, 137 mM sodium chloride, and 10 mM phosphate buffer at pH 7.5 in a conventional quartz cell.

3.3. Fluorescence Spectroscopy
Intrinsic fluorescence was determined using 2.25 μM of BSA with a path length 1 cm cell at 37 °C. All fluorescence measurements were obtained with a fast-scanning Cary Eclipse Agilent spectrofluorometer (Cary Eclipse, Varian, Australia). The emission spectra were analyzed between 300 and 440 nm, with an excitation wavelength of 280 nm. MTBA concentration was varied from 0-25λ (each λ equal 8.3 μM). The Stern-Volmer constant (K_{sv}) is evaluated to the quenching efficiency of MTBE. This parameter was calculated using the equation of $F_0/F = 1 + [MTBE]K_{sv}$, where F_0 and F are the emission intensities in the absence and the presence of the MTBE, respectively (23).

3.4. Circular Dichroism (CD) Spectroscopy
In the presence of MTBE, changes in the secondary structure of BSA were observed. CD spectroscopy measurements were performed in an Aviv 215 spectropolarimeter utilizing a 1 mm path length cell in the far UV-CD region (195-250 nm). CD spectra were performed in the fixed concentration of BSA (2.25

μM) with different concentrations of MTBE 0-20λ concentrations (each λ equal 8.3 μM), at 37 °C. Far UV-CD measurements of samples are performed using Aviv, Model 215, and USA spectrometer. The spectra were recorded in a 1 mm quartz cell and step size of 1 nm with three or two accumulations.

3.5. Thermodynamics Parameters

The fluorescence emission spectra of the samples were examined at two different temperatures (298.15 and 310.15 K) to determine the thermodynamic parameters (ΔH, ΔS, ΔG). The van't Hoff equation was used to compute ΔH:

$$\Delta H = R \ln (K_{b(T2)}/K_{b(T1)}) / (1/T_1 - 1/T_2) \tag{1}$$

$K_{b(T2)}$ and $K_{b(T1)}$ are the binding constants at the first and second temperatures, respectively, and R is the universal gas constant (8.3145 j/k.mol). The thermodynamic equation was used to calculate ΔG and ΔS:

$$\Delta G = \ln K_{b(T)} \ (-RT) \tag{2}$$

$$\Delta S = -(\Delta G - \Delta H)/T \tag{3}$$

3.6. Molecular Dynamics Simulation

The initial coordinates of BSA were obtained from its crystal structure (PDB ID: 3VO3) (24), and the MTBE structure was taken from PubChem CID:15413 (http://pubchem.ncbi.nlm.nih.gov/) (**Fig. 1**). MD simulations were performed with GROMACS, version 5.1.2 simulation package using the GROMOS 96-54a7 force field. Water molecules of the crystal structure were removed. The BSA was simulated in pure water. BSA and BSA-MTBE complex were immersed in a 90000-molecule cubic box water (with dimensions $10\times10\times10$ nm) using the simple point charge (SPC) water molecules. Chloride and sodium ions were used to neutralize the systems. Using the Berendsen method with 0.1 and 0.5 τps, the temperature and pressure were held near the target values (300 k and 1 bar, respectively) (25). The LINCS algorithm was used to constrain the length of covalent bonds (26). A short-range spherical cut-off 1 nm was applied for all nonbonded interactions. The Particle Mesh Ewald (PME) approach was used to calculate the long-range interactions (27). The steepest descent approach was employed to reduce the energy consumption of the MD simulation systems. The conventional (NVT) ensemble was run for 0.5 ns after energy reduction.
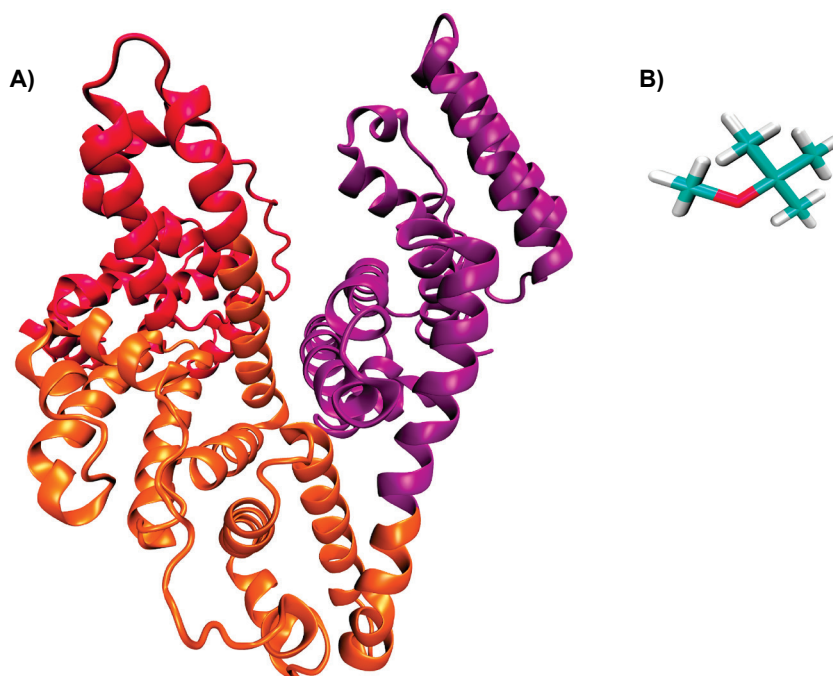
Figure 1. A) Bovine Serum Albumin (Domain I; red, domain II; orange, domain III; purple).
B) Methyl-tert-butyl ether (MTBE)

All systems were then equilibrated using an isothermal-isobaric (NPT) for 1 ns. The simulation length for each BSA-MTBE and free BSA system was 200 ns (28). Given that the allowable amount for MTBE is 15 µg maximum per liter by Iranian national standard and 40 µg per liter for the US, the necessary calculations were performed, and it was found that for each box of 90000-water molecules, a much smaller number than one MTBE molecule was obtained. Since this number was not mathematically practicable, one molecule was selected, equivalent to a concentration of 616 µM (54.3 mg. L^{-1}) in the box. The BSA concentration should be 41.7 g. L^{-1} is performed. Due to this study's specific conditions, the size of the protein and the smallness of the ligand selected were much greater than that of the *in vitro* concentration. However, this selective amount of simulation was also performed in the laboratory phase to make a reasonable comparison. The minimization was completed when the root-mean-square deviation (RMSD) achieved a maximum value of 0.30. The binding mechanism of MTBE with bovine serum albumin was investigated using molecular docking. Simulations of free BSA and BSA-MTBE were carried out.

3.7. Molecular Docking

In this work, the AutoDock software (Version 4.2.6) was utilized to simulate MTBE's binding site upon interactions with BSA. In general, the Lamarckian genetic algorithm (LGA) was applied for the local search (Solis and Wets method). Kollman partial charges and polar hydrogens were added to the BSA structure during the simulation. Then in the AutoDock tools package, the partial atomic charges were calculated using the Gasteiger-Marsili method, and after merging non-polar hydrogens, rotatable bonds were assigned (29). The number of grid points in the x, y, and z axes was 126 Å ×126 Å ×126 Å. The distance between the two connecting grid points was 0.375 Å (roughly a quarter of a carbon-carbon single bond). A structure with the lowest energy content and the best binding site was selected. Using discovery studio and ligand scout software, hydrogen bonds and hydrophobic interaction sites were assessed with their binding partner.

4. Results

### 4.1. UV-vis Absorption Spectra Investigation

BSA is composed of 585 amino acid residues, and it has several aromatic amino acids. BSA has two absorption bands at near 220 nm, which is related to α-helix structure and represents the conformation of BSA, and 280 nm, which is linked to the π–π* transition of the aromatic residues such as Trp, Tyr, and Phe residues (30, 31). The UV-visible spectra of BSA solutions in the presence of MTBE are shown in **Figures 2A** and **B**. Electronic absorption spectroscopy is an impressive method to analyze the binding mode of protein and small molecules. To record the possibility of MTBE interaction with BSA, spectroscopic titration of different concentrations of MTBE with a constant BSA concentration has been performed. The result shows that MTBE could affect the BSA structure immediately (**Fig. 2A**). The association remains the same after a 3-hour incubation period (**Fig. 2B**). The intensity of the two bands has risen, indicating that the hydrophobicity around aromatic residues has decreased and BSA's -helical content has grown. Consequently, our findings suggest that MTBE may affect the microenvironment of aromatic acid residues in BSA.

4.2. Intrinsic Fluorescence Study

Fluorescence spectroscopy is a high-sensitivity technique for the protein's structural transition in interaction with different ligands (32). BSA consists of several aromatic residues that contribute to the BSA intrinsic fluorescence absorption (Trp, Tyr, Phe) (33). Two tryptophan residues, Trp-134, located on the surface of subdomain IB, and Trp-212, located within the hydrophobic binding pocket of subdomain IIA, possess intrinsic fluorescence in BSA (21, 34). The fluorescence emission spectrum of BSA in the presence of various concentrations of MTBE is given in **Figure 2C**. BSA has a strong fluorescence emission peak approximately at 350 nm. It was discovered that the emission intensity of BSA increases at low concentrations and decreases somewhat with rising MTBE concentrations, with no discernible emission wavelength change. This trend represents the decreasing BSA intrinsic fluorescence owing to interaction with MTBE. The solution property changed in terms of increasing MTBE concentrations. The same alternation caused the micro-environment around residues to have intrinsic fluorescence, and residue with innate fluorescence intensity could fluctuate freely. Fluorescence emission decreased owing to this increased residue moving.

The Stern–Volmer plot showed in **Figure 2D**. The
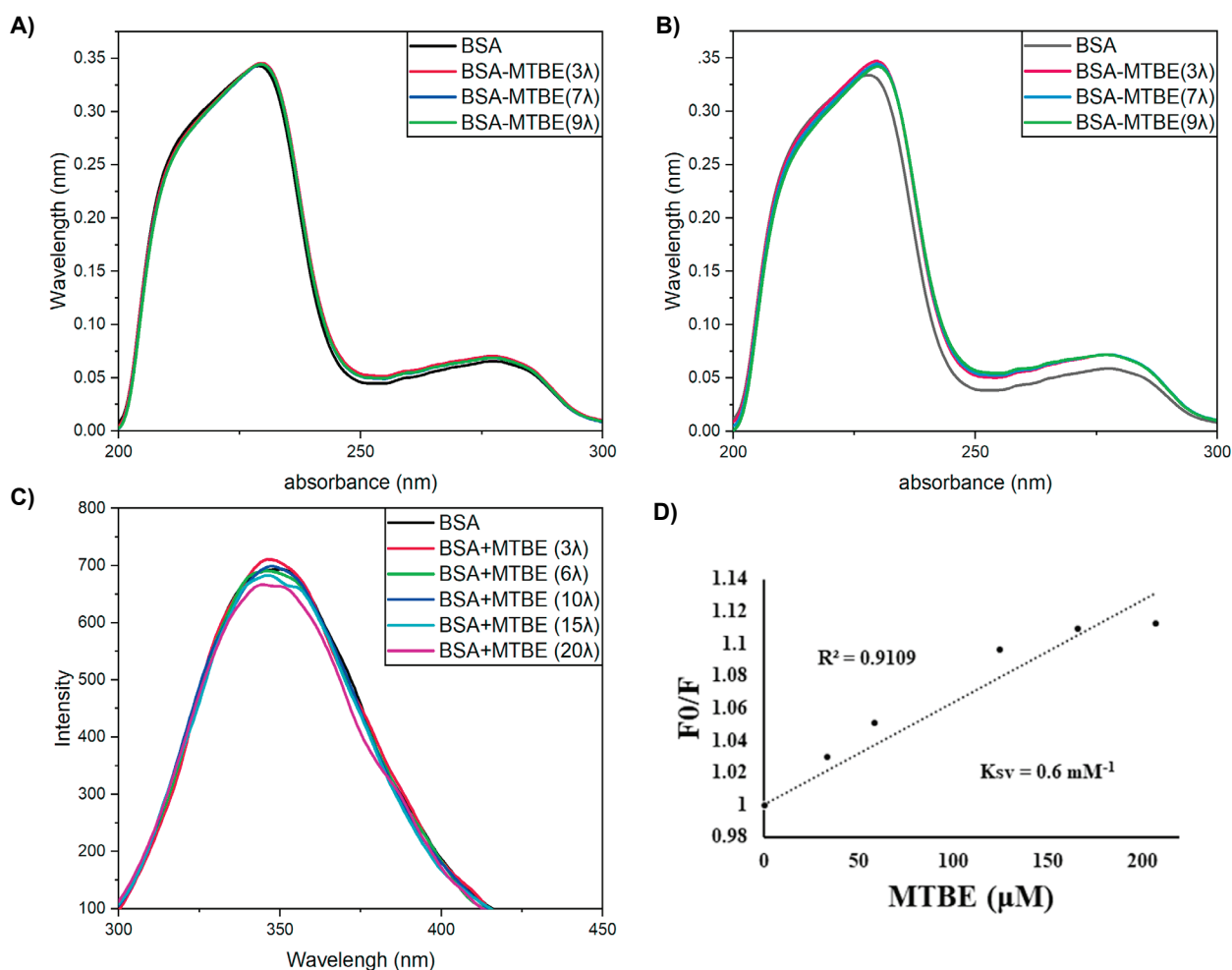
Figure 2. UV-Vis and intrinsic fluorescence spectra of BSA (2.25 µM) in the presence of different MTBE concentrations at 37 °C. Samples are prepared in PBS buffer, pH 7.4. **A)** UV-Vis spectra of MTBE-BSA interaction without incubation. **B)** UV-Vis spectra of MTBE-BSA interaction after 3-hour incubation. **C)** Fluorescence emission spectra of BSA in the presence of various concentrations of MTBE. **D)** The Stern-Volmer plot of BSA-MTBE interaction.

Stern-Volmer plot of BSA-MTBE illustrates that the quenching of interaction of BSA by MTBE is in good agreement (R^2 = 0.91). The Stern-Volmer constant was determined from the slope of the linear curve and equaled 0.6 mM^{-1}. These results in a decrease in the fluorescence intensity, and the high K_{sv} value of the MTBE shows that MTBE could interact with BSA.

The thermodynamic characteristics of the BSA and MTBE interaction were determined at two temperatures, 298.15 and 310.15 K (**Table 1**). Considering ΔH and ΔS are more significant than zero, it is concluded that hydrophobic interactions are the primary driving forces for the BSA-MTBE binding.

4.3. Circular Dichroism Measurement

CD spectroscopy analysis is used to accurately evaluate the secondary structural changes of BSA under different MTBE concentrations. Far UV-CD spectra of BSA in the absence and presence of MTBE are given in **Figure 3**. For α-helix-rich protein like BSA, CD spectra show two negative peaks at 208 and 222 nm (35). Studies reported that native BSA has around 65% of α-helical secondary structure content (23). The CD results indicated that MTBE increases the content of the secondary structure in low concentrations (**Table 2, Fig. 3**). Therefore, by increasing the MTBE concentration, the secondary structure content is decreased.

Table 1. Thermodynamics parameters of BSA-MTBE interaction.

T (K)	ΔH (Kj.mol⁻¹)	ΔG (Kj.mol⁻¹)	ΔS (j.mol⁻¹)	Ka(L.mol⁻¹)10³	Interference force
298.15	106.674	-3.198	0.369	3.65	**Hydrophobic interaction (ΔH<0, ΔS<0)**
310.15	106.674	-8.003	0.369	22.3	
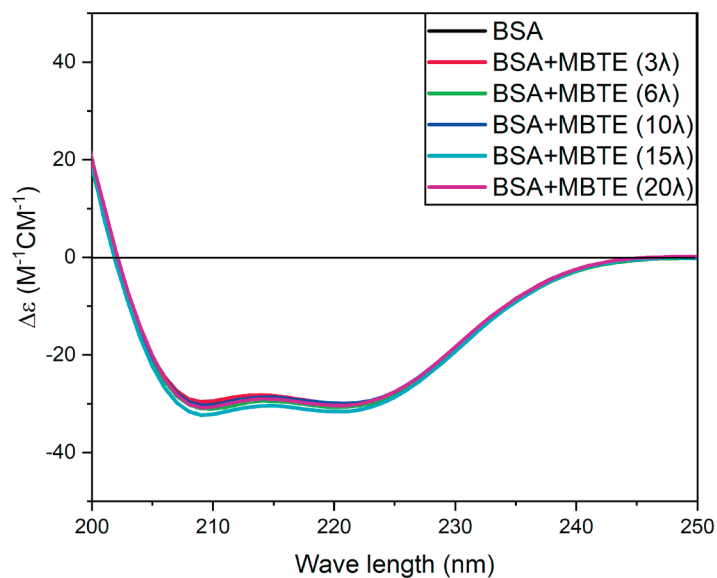
Figure 3. Circular dichroism (CD) spectra of BSA in the presence of different effective concentrations of MTBE compared with naked protein. The Δε intensity measurement shows the increasing MTBE concentration was maintained the BSA secondary protein structure in the two critical wavelength points (208 and 222 nm).

**Table 2.** Secondary structure contents of BSA at different concentrations of MTBE.

Systems	% α-helix	%β-Turn	%Parallel	%Antiparallel	% Random coil
BSA	66.5	11.7	3.6	1.4	16.8
BSA-MTBE(3λ)	69.4	11.5	3.5	1.3	14.3
BSA-MTBE(6λ)	70.2	11.3	3.1	1.2	14.2
BSA-MTBE(10λ)	69.2	11	2.4	1.4	16
BSA-MTBE(15λ)	71.8	9.5	1.5	0.9	16.3
BSA-MTBE(20λ)	65.1	9	2	0.9	17.0

This, like fluorescence results, shows that at low concentrations, MTBE increases the structural stability and has a different effect at higher concentrations.

4.4. Molecular Dynamics Analysis

MD modeling has the potential to reveal minute information regarding protein-small molecule interactions. MD data might reveal structural alterations and system stability that a protein may experience in the presence of tiny compounds (36). To investigate the conformational dynamics of MTBE interaction with BSA, 200 ns long MD simulations were done at a temperature of 300 K. The structural stability and energetic features of BSA-MTBE interaction were

monitored based on the time course of the C_α root-mean-square deviation (RMSD) concerning to their initial conformation. The RMSD values for free BSA and BSA-MTBE complexes during MD simulations are shown in **Figure 4A**. The RMSD of BSA-MTBE is almost stable and fluctuates between 0.4 and 0.7 nm. The fluctuation of BSA-MTBE is approximately more stable after 100 ns. However, free BSA fluctuates between 0.3 nm and 0.6 nm with a slightly variable pattern throughout the 200 ns simulation. The RMSD value of free BSA represents different RMSD values than the BSA-MTBE complex; therefore, these results indicate that the conformational change occurred during the BSA-MTBE interaction. The root-mean-
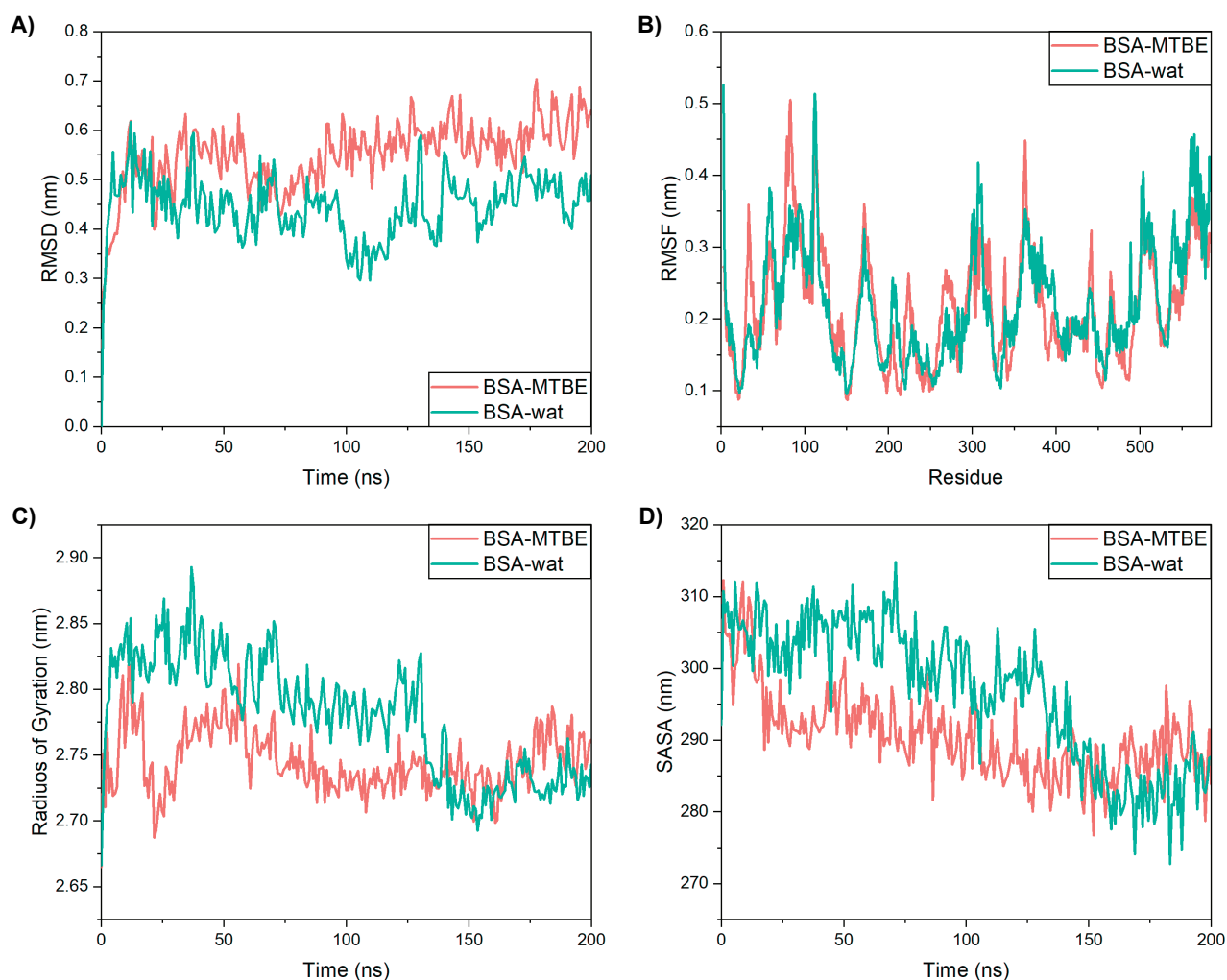
Figure 4. Molecular dynamics results of free BSA and MTBE-BSA interaction in 200 ns simulation. **A)** Root mean squared deviation (RMSD) of Cα atoms as a function of time was calculated. **B)** Comparison of root mean square fluctuation (RMSF) values. **C)** Comparison of the radius of gyration (R_g) values. **D)** Comparison of solvent accessible surface area (SASA) values.

square fluctuations (RMSF) of protein backbone atoms were determined for the free BSA and the BSA-MTBE complex. During MD trajectories, the RMSF calculates the average atomic mobility. The more flexible residues of protein structure show higher RMSF values (37). As shown in **Figure 4B**, clearly different flexibilities in the binding sites of BSA in the presence and absence of MTBE are observed. The binding sites in subdomains IA and IB are more flexible when MTBE interacts with BSA. In the lack of MTBE, IIB, IIIA, and IIIB subdomains are more flexible. This pattern shows that the structural stability of BSA alters during the MTBE interaction.

Figure 4C shows the radius gyration of both free BSA and BSA-MTBE. The compactness of a protein can be determined through the radius of gyration (R_g), which expressed that the lesser the R_g more compact the molecule (38). The lower R_g result indicates that BSA-MTBE has a compact structure throughout MD simulation. The stabilization of the BSA-MTBE complex is illustrated in the consistency of R_g values after 30 ns. Moreover, solvent accessibility surface area

(SASA) for the proteins was also measured and depicted in **Figure 4D**. The decreasing SASA values represent relative compactness. The lower SASA result indicates that BSA-MTBE has a compact structure throughout MD simulation and obtains from R_g and RMSF.

4.5. Molecular Docking Results

To investigate the binding site of BSA to MTBE, molecular docking was performed. The low energy binding site with the best fits MTBE is shown in **Figure 5**. The docking result indicates that a binding site on BSA has a perfect binding affinity for MTBE; the following residues interact with MTBE: Val40, Lys132, Lys131, Phe36, Trp134, Lys20, Asn44, and Val34 are located in IA and IB subdomains (**Fig. 5A, 5B**). MTBE binds to BSA with a binding energy of -6.3 kcal/mol. More specifically, subdomain IA and IB have more RMSF values. It seems that this fluctuation is related to MTBE interaction with this region of BSA. Trp134 is involved in MTBE interaction hence decrease in fluorescence intensity occurs during these interactions and could affect the microenvironment polarity of Trp134 in subdomain
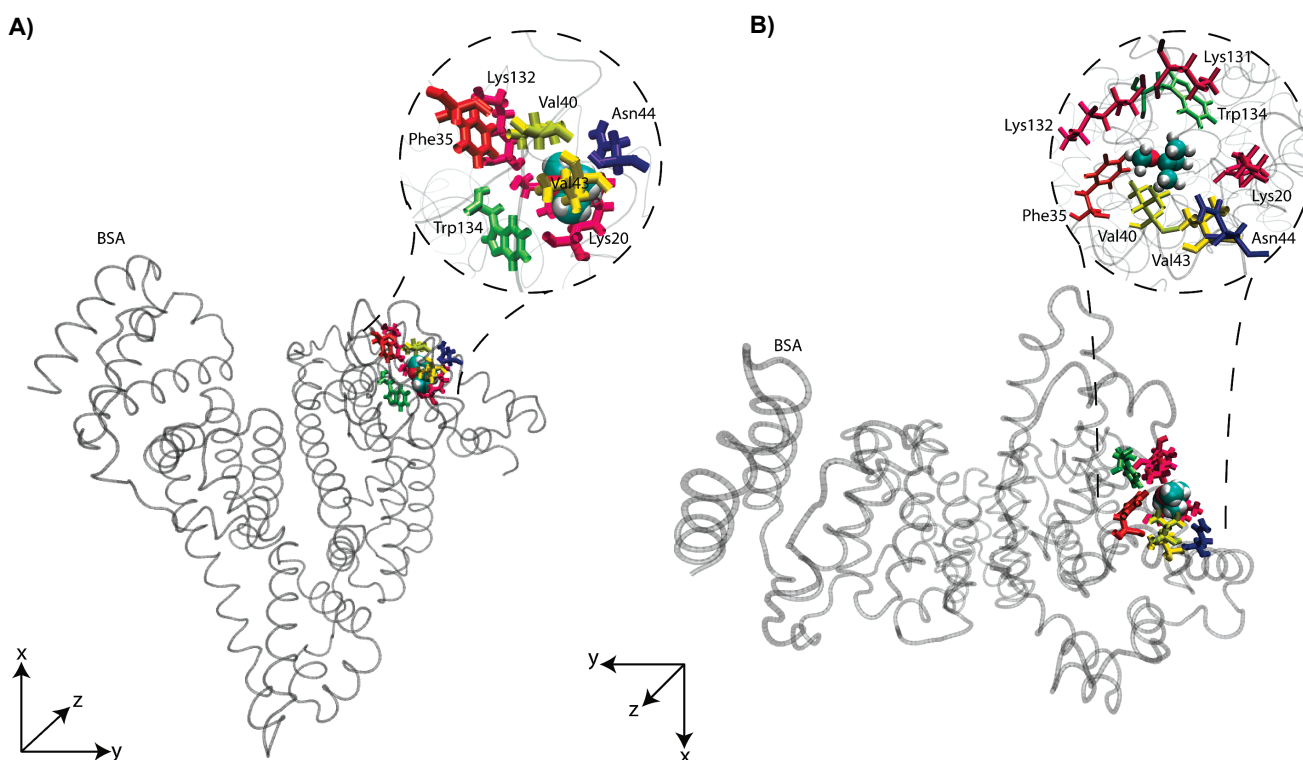
Figure 5. Interaction between BSA and MTBE based on the docking result. The residues have a significant role in the binding process of MTBE-BSA interaction in two different aspects. A) XY axis. B) Z axis. Residues like Val40, Lys131, Phe134, Lys20, Asn44, and Val34 are located in IA and IB subdomain corporate to interact the MTBE with -6.3 Kcal.mol⁻¹ free binging energy.

84

Iran. J. Biotechnol. July 2022;20(3): e3111

IB. According to molecular docking and MD modeling, the hydrophobic head of MTBE (methyl) interacts with the hydrophobic cavity of IA and IB of the BSA protein, causing a structural alteration in BSA. Compared to free BSA, MTBE-BSA is more stable and has a compact structure.

5. Discussion

In order to improve air quality, the production and use of fuel oxygenate as MTBE has increased since the early 1990s. The prevalent use of MTBE in gasoline has been accompanied by widespread release into the environment. MTBE is a comparatively unreactive compound in the environment (39). MTBE can pollute the environment, quickly enter the blood, and significantly affect the proteins. The previous study showed that MTBE interacts with hemoglobin, perturbs its structure and function, and degrades heme; therefore, adversely affects oxygen affinity and transportation (17). Besides, MTBE could alter insulin structure, form insulin aggregation, and generate reactive oxygen species (14). The *in vivo* studies illustrated that MTBE has genotoxic potential and forms adducts with DNA (40). Serum albumins are a key component of blood plasma because they aid in the binding and transporting of a wide range of exogenous and endogenous chemicals, such as hormones, fatty acids, and medicines (22). As a result, concerns about potential inhalation health effects and, more recently, increased concerns about water contamination of the side effects of this environmental pollutant on human health were investigated.

6. Conclusion

The fluorescence spectroscopy results show that interaction between widespread environmental pollutant MTBE and BSA decreases fluorescence emission intensity in higher concentrations. Furthermore, UV-vis and CD results indicate the binding interaction of MTBE with BSA by an increase in α-helix of the secondary structure in low concentrations. At the MTBA doses utilized in this experiment, compression occurs in the protein structure. The hydrophobic interaction was the primary force between MTBE-BSA complexes, according to the thermodynamic characteristic. MD simulation and docking consequences confirmed experimental results. Our result demonstrated that the BSA secondary structure is maintained in low MTBE concentration; however, it's detrimental in higher concentrations.

Conflict of Interests

The authors declare that they have no conflict of interest

References

1. Lee EH, Cho KS. Effect of substrate interaction on the degradation of methyl tert-butyl ether, benzene, toluene, ethylbenzene, and xylene by Rhodococcus sp. *J Hazard Mater.* 2009;**167**(1-3):669-674. doi: 10.1016/j.jhazmat.2009.01.035

2. Joshi G, Schmidt R, Scow KM, Denison MS, Hristova KR. Effect of benzene and ethylbenzene on the transcription of methyl-tert-butyl ether degradation genes of Methylibium petroleiphilum PM1. *Microbiology.* 2016;**162**(9):1563-1571. doi: 10.1099/mic.0.000338

3. Intrchom W, Roy S, Mitra S. Removal and recovery of methyl tertiary butyl ether (MTBE) from water using carbon nanotube and graphene oxide immobilized membranes.*Nanomaterials.* 2020;**10**(3):578. doi: 10.3390/nano10030578

4. Squillace PJ, Pankow JF, Korte NE, Zogorski JS. Review of the environmental behavior and fate of methyl tert-butyl ether. *Environ Toxicol Chem.* An International Journal. 1997;**16**(9):1836-1844. doi: 10.1002/etc.5620160911

5. Kucharzyk KH, Rectanus HV, Bartling CM, Rosansky S, Minard-Smith A, Mullins LA, et al. Use of omic tools to assess methyl tert-butyl ether (MTBE) degradation in groundwater. *J Hazard Mater.* 2019;**378**:120618. doi: 10.1016/j.jhazmat.2019.05.011

6. Levchuk I, Bhatnagar A, Sillanpää M. Overview of technologies for removal of methyl tert-butyl ether (MTBE) from water. *Sci Total Environ.* 2014;**476**:415-433. doi: 10.1016/j.scitotenv.2014.01.037

7. Ahmadian M, Pirsaheb M, Janjani H, Hossaini H. Ultraviolet activated persulfate based AOP for MTBE decomposition in aqueous solution. *Desalin Water Treat..* 2019;**161**:269-274. doi: 10.5004/dwt.2019.24310

8. Belpoggi F, Soffritti M, Filippini F, Maltoni C. Results of long-term experimental studies on the carcinogenicity of methyl tert-butyl ether. *Ann N Y Acad Sci.* 1998;**837**:77-95. doi: 10.1111/j.1749-6632.1997.tb56865.x

9. Bird M, Burleigh-Flayer H, Chun J, Douglas J, Kneiss J, Andrews L, editors. Oncogenicity studies of inhaled methyl tertiary-butyl ether (MTBE) in CD-1 mice and F-344 rats. Journal of Applied Toxicology: An International Forum Devoted to Research and Methods Emphasizing Direct Clinical, Industrial and Environmental Applications; 1997: *Wiley Online Library.* doi: 10.1002/(sici)1099-1263(199705).

10. Daughtrey WC, Gill MW, Pritts IM, Douglas JF, Kneiss JJ, Andrews LS, editors. Neurotoxicological evaluation of methyl tertiary-butyl ether in rats. Journal of Applied Toxicology: An International Forum Devoted to Research and Methods Emphasizing Direct Clinical, Industrial and Environmental Applications; 1997: *Wiley Online Library.* doi: 10.1002/(sici)1099-1263(199705).

11. Johanson G, Nihlén A, Löf A. Toxicokinetics and acute effects of MTBE and ETBE in male volunteers. *Toxicol. Lett.* 1995;**82**(83):713-718. doi: 10.1016/0378-4274(95)03589-3

12. Ahmed FE. Toxicology and human health effects following exposure to oxygenated or reformulated gasoline. *Toxicol Lett.*

2001; **123**(2-3):89-113. doi: 10.1016/S0378-4274(01)00375-7

13. Guerrero-Barajas C, Alanís-Sánchez B, Flores-Ortiz C, Cruz-Maya J, Jan-Roblero J. Enhanced removal of methyl tert-butyl ether by yeast extract supplementation to a bacterial consortium. *Revista Mexicana de Ingeniería Química*. 2019;**18**(2):589-604. doi:10.24275/uam/izt/dcbi/revmexingquim/2019v18n2/Guerrero

14. Valipour M, Maghami P, Habibi-Rezaei M, Sadeghpour M, Khademian MA, Mosavi K, *et al.* Interaction of insulin with methyl tert-butyl ether promotes molten globule-like state and production of reactive oxygen species. *Int J Biol Macromol*. 2015;**80**:610-614. doi: 10.1016/j.ijbiomac.2015.07.030

15. Sun Y, Wei S, Yin C, Liu L, Hu C, Zhao Y, *et al.* Synthesis and spectroscopic characterization of 4-butoxyethoxy-N-octadecyl-1, 8-naphthalimide as a new fluorescent probe for the determination of proteins. *Bioorg Med Chem Lett*. 2011;**21**(12):3798-3804. doi: 10.1016/j.bmcl.2011.04.026

16. Amberg A, Rosner E, Dekant W. Toxicokinetics of methyl tert-butyl ether and its metabolites in humans after oral exposure. *Toxicol. Sci.* 2001;**61**(1):62-67. doi: 10.1093/toxsci/61.1.62

17. Valipour M, Maghami P, Habibi-Rezaei M, Sadeghpour M, Khademian MA, Mosavi K, *et al.* Counteraction of the deleterious effects of reactive oxygen species on hemoglobin structure and function by ellagic acid. *Journal of Luminescence*. 2017;**182**:1-7. doi: 10.1016/j.jlumin.2016.10.003

18. Al-Harthi S, Lachowicz JI, Nowakowski ME, Jaremko M, Jaremko Ł. Towards the functional high-resolution coordination chemistry of blood plasma human serum albumin. *J inorganic biochem*. 2019;**198**:110716. doi: 10.1016/j.jinorgbio.2019.110716

19. Kandagal P, Ashoka S, Seetharamappa J, Shaikh S, Jadegoud Y, Ijare OB. Study of the interaction of an anticancer drug with human and bovine serum albumin: spectroscopic approach. *J Pharm Biomed Anal*. 2006;**41**(2):393-399. doi: 10.1016/j.jpba.2005.11.037

20. Tian Z, Zang F, Luo W, Zhao Z, Wang Y, Xu X, *et al.* Spectroscopic study on the interaction between mononaphtha-limide spermidine (MINS) and bovine serum albumin (BSA). *J Photochem Photobiol B Biol*. 2015;**142**:103-109. doi: 10.1016/j.jphotobiol.2014.10.013

21. PBourassa P, Hasni I, Tajmir-Riahi H. Folic acid complexes with human and bovine serum albumins. *Food Chem.* 2011;**129**(3):1148-1155. doi: 10.1016/j.foodchem.2011.05.094

22. Ju P, Zhang Y, Ding J, Zheng Y, Wang S, Jiang F, *et al.* New insights into the toxic interactions of polyvinyl chloride microplastics with bovine serum albumin. *Environ. Sci Pollut Res Int.* 2021;**28**(5):5520-5531. doi: 10.1007/s11356-020-10707-1

23. Ali MS, Al-Lohedan HA. Deciphering the interaction of procaine with bovine serum albumin and elucidation of binding site: A multi spectroscopic and molecular docking study. *J Mol Liq.* 2017;**236**:232-240. doi: 10.1016/j.molliq.2017.04.020

24. Majorek KA, Porebski PJ, Dayal A, Zimmerman MD, Jablonska K, Stewart AJ, et al. Structural and immunologic characterization of bovine, horse, and rabbit serum albumins. *Mol Immunol*. 2012;**52**(3-4):174-182. doi: 10.1016/j.molimm.2012.05.011

25. Berendsen HJ, van der Spoel D, van Drunen R. GROMACS: A message-passing parallel molecular dynamics implementation. *Computer Physics Communications*. 1995;**91**(1-3):43-56. doi: 10.1016/0010-4655(95)00042-e

26. Berweger CD, van Gunsteren WF, Müller–Plathe F. Finite element interpolation for combined classical/quantum mechanical molecular dynamics simulations. *J computation chem.* 1997;**18**(12):1463-1472. doi: 10.1002/(SICI)1096-987X(199709)

27. Darden T, York D, Pedersen L. Particle mesh Ewald: An N-log (N) method for Ewald sums in large systems. *J Chemical Physics*. 1993;**98**(12):10089-10092. doi: 10.1063/1.464397

28. Noordadi M, Mehrnejad F, Sajedi RH, Jafari M, Ranjbar B. The potential impact of carboxylic-functionalized multi-walled carbon nanotubes on trypsin: A Comprehensive spectroscopic and molecular dynamics simulation study. *PLoS One*. 2018; **13**(6):e0198519. doi: 10.1371/journal.pone. 0198519

29. Gasteiger J, Marsili M. Iterative partial equalization of orbital electronegativity-a rapid access to atomic charges. *Tetrahedron*. 1980;**36**(22):3219-3228. doi: 10.1016/0040-4020(80)80168-2

30. Banipal TS, Kaur N, Banipal PK. Binding studies of caffeine and theophylline to bovine serum albumin: Calorimetric and spectroscopic approach. *J Mol Liq.* 2016;**223**:1048-1055. doi: 10.1016/j.molliq.2016.09.034

31. Shi J-h, Pan D-q, Jiang M, Liu T-T, Wang Q. In vitro study on binding interaction of quinapril with bovine serum albumin (BSA) using multi-spectroscopic and molecular docking methods. *J Biomolecular Structure and Dynamics*. 2017;**35**(10):2211-2223. doi: 10.1080/07391102.2016.1213663

32. Roy A, Seal P, Sikdar J, Banerjee S, Haldar R. Underlying molecular interaction of bovine serum albumin and linezolid: A biophysical outlook. *J Biomol Struct Dyn*. 2018;**36**(2):387-397. doi: 10.1080/07391102.2017.1278721

33. Ghisaidoobe AB, Chung SJ. Intrinsic tryptophan fluorescence in the detection and analysis of proteins: a focus on Förster resonance energy transfer techniques. *Int J Mol Sci.* 2014;**15**(12):22518-22538. doi: 10.3390/ijms151222518

*34. *Suryawanshi VD, Walekar LS, Gore AH, Anbhule PV, Kolekar GB. Spectroscopic analysis on the binding interaction of biologically active pyrimidine derivative with bovine serum albumin. *J Pharm Anal*. 2016;**6**(1):56-63. doi: 10.1016/j.jpha.2015.07.001

35. Shamsi A, Ahmed A, Bano B. Probing the interaction of anticancer drug temsirolimus with human serum albumin: Molecular docking and spectroscopic insight. *J Biomol Struct Dyn*. 2018;**36**(6):1479-1489. doi: 10.1080/07391102.2017.1326320

36. Ahmed MF, Molla MR, Saha M, Shahriar I, Rahman MS, Halim MA, *et al*. Aggregation behavior of cetyldimethyl-ethylammonium bromide under the influence of bovine serum albumin in aqueous/electrolyte solutions at various temperatures and compositions: conductivity and molecular dynamics study. *RSC Advances*. 2019;**9**(12):6556-6567. doi: 10.1039/C9RA00070D

37. Rahban M, Salehi N, Saboury AA, Hosseinkhani S, Karimi-Jafari MH, Firouzi R, *et al.* Histidine substitution in the most flexible fragments of firefly luciferase modifies its thermal stability. *Arch Biochem Biophys*. 2017;**629**:8-18. doi: 10.1016/j.abb.2017.07.003

38. MIu L, Bogatyreva N, Galzitskaia O. Radius of gyration is indicator of compactness of protein structure. *Molecular Biology.* 2008;**42**(4):623-628. doi: 10.1134/s0026893308040195

39. Lien H-L, Zhang W-X. Removal of methyl tert-butyl ether (MTBE) with Nafion. *J. Hazard. Mater.* 2007;**144**(1-2):194-199. doi: 10.1016/j.jhazmat.2006.10.004

40. Ghasemi S, Ahmadi F. The study of binding of methyl tert-butyl ether to human telomeric G-quadruplex and calf thymus DNA by gas chromatography, a thermodynamic discussion. *J Chromatogr B Analyt Technol Biomed Life Sci.* 2014;**971**:112-119. doi: 10.1016/j.jchromb.2014.09.011